Long-Path Quantum Cascade Laser–Based Sensor for Methane Measurements

ANNA P. M. MICHEL[a]

Mid-Infrared Technologies for Health and the Environment, Princeton University, Princeton, New Jersey

DAVID J. MILLER,[b] KANG SUN,[c] LEI TAO,[d] LEVI STANTON,[e] AND MARK A. ZONDLO

Mid-Infrared Technologies for Health and the Environment, and Department of Civil and Environmental Engineering, Princeton University, Princeton, New Jersey

(Manuscript received 15 January 2016, in final form 26 August 2016)

ABSTRACT

A long-path methane (CH_4) sensor was developed and field deployed using an 8-μm quantum cascade laser. The high optical power (40 mW) of the laser allowed for path-integrated measurements of ambient CH_4 at total pathlengths from 100 to 1200 m with the use of a retroreflector. Wavelength modulation spectroscopy was used to make high-precision measurements of atmospheric pressure–broadened CH_4 absorption over these long distances. An in-line reference cell with higher harmonic detection provided metrics of system stability in rapidly changing and harsh environments. The system consumed less than 100 W of power and required no consumables. The measurements intercompared favorably (typically less than 5% difference) with a commercial in situ methane sensor when accounting for the different spatiotemporal scales of the measurements. The sensor was field deployed for 2 weeks at an arctic lake to examine the robustness of the approach in harsh field environments. Short-term precision over a 458-m pathlength was 10 ppbv at 1 Hz, equivalent to a signal from a methane enhancement above background of 5 ppmv in a 1-m length. The sensor performed well in a range of harsh environmental conditions, including snow, rain, wind, and changing temperatures. These field measurements demonstrate the capabilities of the approach for use in detecting large but highly variable emissions in arctic environments.

1. Introduction

Atmospheric methane (CH_4) is a potent greenhouse gas that is directly responsible for approximately 21% of the total anthropogenic radiative forcing since preindustrial times and has a global warming potential 28 times that of carbon dioxide (CO_2) over a 100-yr time horizon (IPCC 2013; Montzka et al. 2011). Methane also contributes to tropospheric ozone formation and impacts air quality (Isaksen et al. 2011). Global annual mean CH_4 mixing ratios have been increasing in recent years (1803 ± 2 ppbv) following a temporary leveling of mixing ratios in the late 1990s (IPCC 2013; Rigby et al. 2008; Isaksen et al. 2011). While the total atmospheric burden of CH_4 is well constrained, many anthropogenic and natural CH_4 emission source pathways are poorly quantified, leading to large uncertainties in the partitioning of different sources (Anderson et al. 2010; Dlugokencky et al. 2011; Montzka et al. 2011). Natural CH_4 sources include wetlands, lakes, permafrost peatlands, and termites (Anderson et al. 2010). Global climate change is accelerating natural CH_4 emissions in arctic regions with organic carbon-rich permafrost (Cole et al. 2007; IPCC 2013). These arctic CH_4 emissions are highly uncertain due to large spatial and temporal variability and a lack of field measurements (Walter et al. 2007; Walter-Anthony and Anthony 2013).

[a] Current affiliation: Applied Ocean Physics and Engineering Department, Woods Hole Oceanographic Institution, Woods Hole, Massachusetts.

[b] Current affiliation: Institute at Brown for Environment and Society, Brown University, Providence, Rhode Island.

[c] Current affiliation: Atomic and Molecular Physics Division, Harvard-Smithsonian Center for Astrophysics, Cambridge, Massachusetts.

[d] Current affiliation: NEC Laboratories America, Princeton, New Jersey.

[e] Current affiliation: Sonoma Technology, Inc., Petaluma, California.

Corresponding author address: Anna P. M. Michel, Applied Ocean Physics and Engineering Department, Woods Hole Oceanographic Institution, 266 Woods Hole Road, MS 7, Woods Hole, MA 02543.
E-mail: amichel@whoi.edu

DOI: 10.1175/JTECH-D-16-0024.1

Ground-based CH_4 measurement techniques will ideally be capable of high precision and stability with high spatial and temporal coverage in remote field environments. Large but highly variable trace gas emissions in space and time are significant in many environments but challenging to capture. Existing techniques include flux chambers or bubble chambers for water surfaces combined with highly precise offline gas chromatography analysis and can provide discrete point measurements in space and time across terrestrial and aquatic regions (Pétron et al. 2012; Farrell et al. 2013; Walter et al. 2007). Suto and Inoue (2010) demonstrated an in situ, portable atmospheric CH_4 point sensor with 30-s-averaged mole fractions varying by ± 2 ppbv CH_4 and long-term stability for over 1 week. However, these point sensor sampling strategies may result in low biases for emission estimates due to undersampling of transient hot spots and require a moving platform for extensive spatial measurements. Eddy covariance flux measurements with closed- or open-path analyzers can quantify CH_4 fluxes over large spatial footprints (Eugster and Pluss 2010; McDermitt et al. 2011; Peltola et al. 2013) but are limited to turbulent conditions and are restricted to homogeneous domains. In situ sensors measure at one point in time and therefore must be translated within or around the area of interest (Garcia-Tigreros Kodovskaa et al. 2016). Emissions can be located precisely, but those located elsewhere at the same time are not readily observed.

While fixed- and mobile-based sensors only probe a small volume of air at any given time, long-path-integrated configurations capture average variability across larger spatial scales simultaneously and can be especially advantageous for high-time-resolution monitoring of spatially averaged heterogeneous hot-spot emissions. Long-path sensors spatially integrate over a distance and thus can capture emissions anywhere along the optical path. A major disadvantage of long-path measurements is that the specific emission locations and distributions within the beam path cannot be identified easily. For cases where total emissions in an area are needed but without the subspatial resolution (or in areas where in situ mobile measurements are impossible), long-path measurements are an ideal approach to determine emissions. For example, changing plume positions due to turbulence from a local source is one application for long-path measurements. Another potential application for long-path measurements is spatially variable greenhouse gas emissions from agricultural soils, wetlands, or aquatic environments. Although long-path measurements cannot achieve high spatial resolution that could be accomplished with a high-density network or in situ point sensors, the large spatial coverage that integrates over hot spots is also important. To be able to look at methane levels in remote field environments, it is important to make both long-term measurements and measurements that cover a significant amount of area.

Remote sensing path-integrated CH_4 measurement configurations have been employed to estimate emission fluxes (Griffith and Galle 2000) and are commonly coupled with inverse dispersion models (Flesch et al. 2007). Open-path Fourier transform infrared (OP/FTIR) spectrometry techniques have shown a precision of 10–20 ppbv CH_4 for 10-s measurements (Griffith and Galle 2000). These systems have been deployed in the field at pathlengths of hundreds of meters for CH_4 emission measurements from agricultural facilities (Childers et al. 2001). Although OP/FTIR instruments are commonly calibrated in the field with calibration spectra or calibration cells, these techniques do not necessarily account for drift within the entire path-integrated sampling volume (Demirgian and Macha 1999; Bacsik et al. 2005). OP/FTIR calibration approaches have not been field tested to evaluate their capabilities for maintaining long-term measurement stability, especially in open-path systems with kilometer-scale pathlengths where sampling volume conditions may be rapidly changing (Demirgian and Macha 1999; Bacsik et al. 2005). Tunable diode laser absorption spectroscopy (TDLAS) CH_4 sensors with near-infrared sources have also been developed for laser scanning applications to detect natural gas leakage (Gibson et al. 2006; Xia et al. 2008) and to measure fugitive emission fluxes (Thoma et al. 2005). TDLAS systems such as the GasFinder MC (Boreal Laser Inc.) have shown ~ 1 ppbv CH_4 precision under laboratory conditions at 1-km round-trip pathlength and have been deployed in the field to measure agricultural CH_4 emissions (Desjardins et al. 2004). Xia et al. (2008) demonstrated diode laser–based CH_4 detection at a minimum detection limit of 1.1 ppm m^{-1} with a 120-m optical pathlength but did not address in situ instrument drift. Brooke et al. (2012) demonstrated 144-km open-path CO_2 measurements with $\sim 4\%$ accuracy across two mountaintops with a low-power diode laser–based occultation technique. Although they claimed the technique is easily extended to CH_4 measurements, the sensor was not calibrated in situ and long-term stability of the retrievals was not quantified.

Trace gas measurements of important species such as methane and nitrous oxide require high precision and high stability as nominal ambient fluctuations away from sources are often well below 1% of the ambient background (e.g., a few ppbv out of 1850 ppbv CH_4). While these measurement requirements are exceeded for

numerous closed-path and open-path in situ sensors, long-path sensing of these gases place additional demands on the sensor development. The long-path requires high optical power to ensure sufficient signal on the detector. Losses of light onto the detector occur from Mie scattering of aerosols; partial beam blocking due to insects and precipitation; degradation of exposed optical surfaces, such as the mirrors and lenses; and beam misalignment due to temperature sensitivities in the optomechanical configuration. Finally, long-path measurements by their nature are exposed to sometimes harsh changes in the environment, such as highly variable temperatures, direct sunlight, wind, precipitation, and dust/insects.

Quantum cascade (QC) lasers (QCLs) address some of the optical concerns by providing reasonably high optical power [tens to hundreds of megawatts (MW) readily available commercially] and probing the fundamental (most sensitive) absorption bands of most trace gas species. In contrast to near-IR diode lasers, mid-IR QC lasers require much higher thermoelectric (TE) current for heat dissipation, leading to uncertainties for commercially packaged QC laser performance in diverse field environments. Even with advances in QC laser packaging, the high power dissipation needed to cool QC lasers is not conducive to large changes in the ambient environment. While QC lasers are now routinely used in trace gas in situ atmospheric sensors, there remain open questions as to their capabilities for detecting at the high precision and high stability necessary for gases such as methane in a long-path arrangement. Open-path-integrated instruments using midinfrared QC laser sources with much higher optical power (1–100 mW) have enabled field deployment at much longer, kilometer scale, pathlengths. Michel et al. (2010) measured ozone in an urban environment with a long-path QC laser–based system, but this gas showed fairly large variability (~10%–100%) such that drifts and precision better than a few percent would not be readily noticeable.

We have developed and field deployed a long-path atmospheric CH_4 sensor using an 8-μm QC laser. This laser provides high optical power (40 mW) while also probing an absorption line of ambient CH_4 that avoids optical saturation at long pathlengths (e.g., if one probed the fundamental 3.3-μm band). Wavelength modulation spectroscopy is used to account for the baselines of nearby absorption features and also provides high-sensitivity detection. An in-line reference cell containing N_2O at reduced pressure is used with multiharmonic detection to provide a measure of system drift in the field. The system was deployed at a remote field site for 2 weeks in Toolik Lake, Alaska, to demonstrate the field precision and performance under challenging arctic conditions and an intercomparison was performed at Princeton University with a LI-COR CH_4 point sensor.

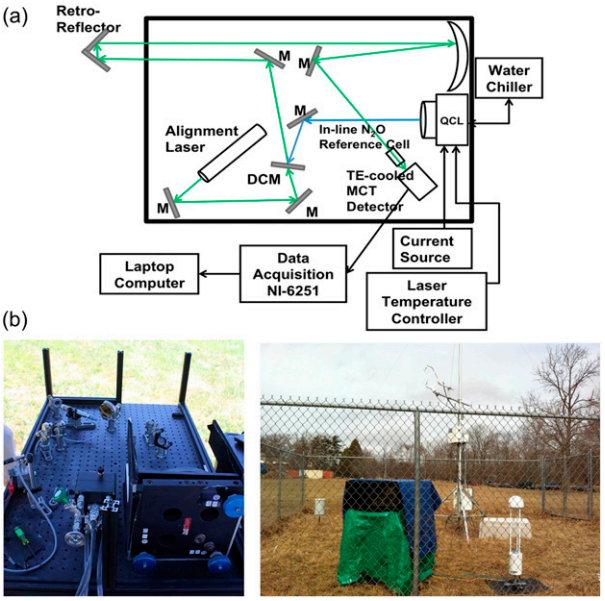

FIG. 1. (a) Schematic of the open-path-integrated QCL-based sensor. The QCL beam is coaligned with a visible laser for long pathlength alignments to a retroreflector. A Newtonian telescope configuration is used with light collection onto a TE-cooled MCT detector. Abbreviations: mirror (M); dichroic mirror (DCM). (b) An open-path-integrated sensor deployed (left) in the field and the sensor (shielded from precipitation) and (right) with a LI-COR LI-7700 CH_4 analyzer during field intercomparison at the Princeton Broadmead site.

2. Sensor design

The path-integrated QC laser–based sensor schematic is shown in Fig. 1a with photos of the field-deployed sensor at the Broadmead Field site in Princeton, New Jersey, in Fig. 1b. A high optical power (~40 mW) 8-μm QC laser (AdTech Optics) was used to probe a CH_4 absorption transition with ~10% absorbance at 300-m optical pathlength. Although relatively short-pathlength CH_4 sensors typically utilize the strongest CH_4 absorption lines at 3.3 μm, these absorption features are not optimal for kilometer-scale pathlengths due to optical saturation. Therefore, we selected the CH_4 absorption line at 8 μm to avoid absorption saturation (Fig. 2).

The QC laser was operated in continuous-wave mode in a laser housing (ILX Lightwave LDM-4872) at 22°C with TE cooling. Recirculated chilled coolant (Koolance coolant; ThermoCube chiller) was used to dissipate heat from the laser housing. The laser current was controlled by a low-noise current source (Wavelength Electronics,

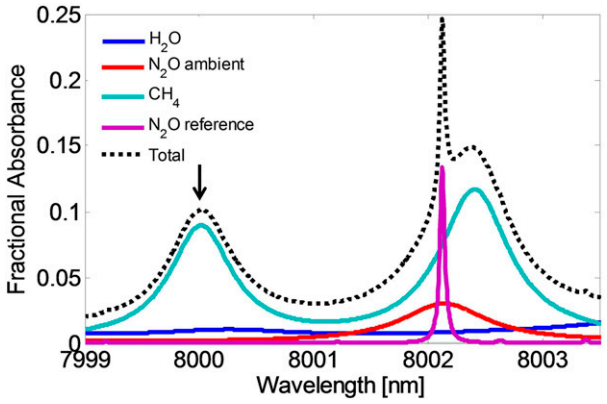

FIG. 2. Direct absorption simulation in the 8-μm region based on the HITRAN (Rothman et al. 2009). The following conditions are used for simulation: 1.9 ppmv CH_4, 325 ppbv N_2O, 390 ppmv CO_2 (all at ambient pressure of 1013 hPa and pathlength of 300 m), and 1% N_2O in N_2 at reduced pressure (50 hPa; 5-cm pathlength). Total absorption is shown by the dotted black line. The arrow indicates the CH_4 absorption line at 8000 nm used for ambient CH_4 detection.

QCL-500) and the laser temperature was regulated by a precision temperature controller (ILX Lightwave LDT5980). A Newtonian telescope was employed to launch and receive the QC laser light with one corner-cube retroreflector (Newport Optics 63.5-mm diameter aperture) placed at a selected distance away from the telescope in a transmitter–retroreflector–receiver configuration (Fig. 1a). A visible (532 nm) laser was coaligned with the infrared beam to facilitate long-distance alignments to the retroreflector. The received light was focused onto a TE-cooled mercury cadmium telluride (MCT) detector (Vigo Systems). A National Instruments data acquisition board (NI-6251) acquired the detector signal, which was transmitted to a laptop computer. The detector signal was processed by a custom Labview-based algorithm that performs multi-harmonic wavelength modulation spectroscopy and real-time spectral fitting of all relevant absorption features (CH_4, N_2O, H_2O) (Tao et al. 2012). Retrieved mole fractions were corrected for water vapor dilution, and air density corrections using meteorological data collected at the detector location were applied to calculate CH_4 dry mixing ratios.

Since open-path measurements are sensitive to changing environmental conditions within the sampling volume, it is essential to maintain instrument stability and account for instrument drifts. Small sensor drifts over time can appear as real mixing ratio fluctuations but may instead originate from sensor system instabilities, including detector or laser temperature fluctuations, electronics temperature dependencies, and optical interference fringing. To account for these drifts, we use an in-line reference N_2O absorption signal that is spectrally offset from the ambient CH_4 absorption signal. Although this in-line technique has previously been demonstrated for open-path atmospheric measurements of other trace gases (Tao et al. 2012; Sun et al. 2013; Miller et al. 2014), we implement this technique in a path-integrated sensor configuration for CH_4 detection at 8 μm. The reference cell was placed in line with the long optical path. As shown in the high-resolution transmission (HITRAN)-simulated spectra (Fig. 2), the sealed N_2O reference cell (1% N_2O in N_2 at a reduced pressure of 50 hPa and 5-cm length) yields stronger absorbance and a narrower line width than the pressure-broadened ambient CH_4 and N_2O absorption signal. While ambient (atmospheric) N_2O and CH_4 would nominally impact the reference signal, the narrow line width of the reference signal and higher harmonic detection minimize this potential interference as discussed below. In addition, atmospheric variability of N_2O is small ($<$1 ppbv out of 325 ppbv) and the pressure-broadened line would not interfere with the N_2O reference signal.

Wavelength modulation spectroscopy (WMS), in which a high-frequency sinusoidal modulation is superimposed on the laser current tuning function, was used for high-sensitivity detection. Linear current tuning was implemented to scan across the spectral features of CH_4 and a reference signal of N_2O (Fig. 2). The laser was scanned across the absorption lines at 100 Hz, and sinusoidal modulation at 40 kHz was applied for WMS.

The detector signal was demodulated at harmonics of the modulation frequency (40 kHz) to minimize laser excess noise by shifting the detection bandwidth to higher frequencies (Schilt et al. 2003). Figure 3 shows the WMS spectra within the laser scan range. The CH_4 absorption line at 8000 nm without spectral interference from N_2O and minimal interference from other atmospheric species (shown by the arrows in Figs. 2 and 3a) was used for ambient CH_4 detection via the second harmonic (2f) signal. The sixth harmonic (6f) signal at 8002 nm was used for detection of the in-line N_2O reference absorption line (discussed below) and was used to normalize the 2f CH_4 absorption signal (Fig. 3b).

The N_2O reference cell concentration was chosen to produce an absorption signal significantly larger than the 6f CH_4 signal for a given long pathlength configuration. Since the N_2O reference cell pathlength (5 cm) was constant when the total long pathlength was changed, absorption was constant at ~25% (Fig. 2). For representative ambient atmospheric conditions (as simulated in Fig. 3b), the CH_4 6f absorption signal was 2.5% of the N_2O reference signal height and the ambient N_2O signal was 0.3% of the reference signal height.

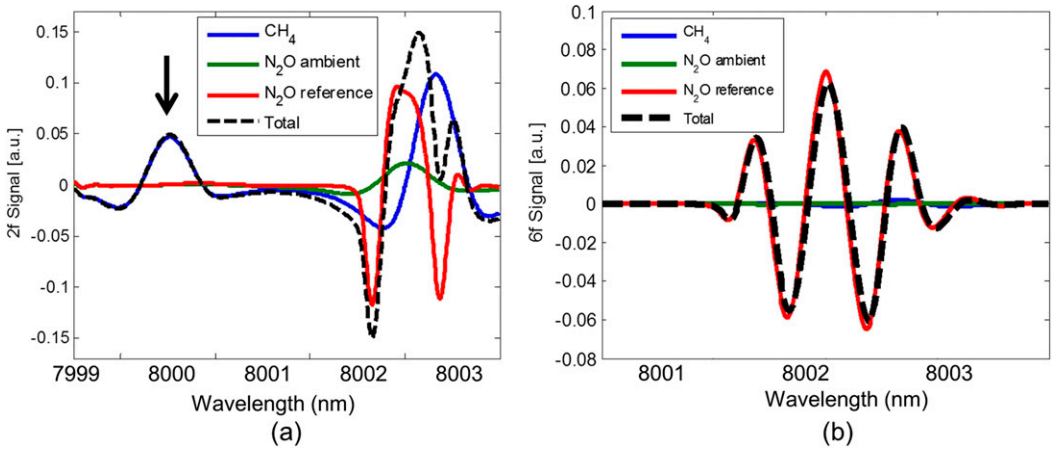

FIG. 3. (a) Second harmonic (2f) spectra simulated using the HITRAN database (Rothman et al. 2009). The ambient signals are at 1000 hPa and N_2O reference signal at 50 hPa (overmodulated) and 5-cm pathlength. The mixing ratios are as follows: 1.9 ppmv CH_4, 325 ppbv ambient N_2O, and 1% N_2O in N_2 (reference). The pathlength simulated for ambient signals is that for the Princeton Broadmead site deployment (240 m). Total absorption is shown by the dotted black line. (b) Sixth harmonic (6f) signal of the same conditions described in (a), showing the isolation of the narrow N_2O reference signal at higher harmonics. The arrow indicates the CH_4 absorption line at 8000 nm used for ambient CH_4 detection.

Because of simultaneous spectral fitting of all absorption lines at 6f, small changes in ambient CH_4 or N_2O have minimal impact on the in-line reference N_2O signal. For very high CH_4 levels, the N_2O reference cell is not necessary for high-precision and stability measurements. Figure 4 shows the 2f CH_4 (1 s) and 6f N_2O reference (30 s) spectra recorded in the field at 458-m total pathlength with real-time simultaneous spectral fitting of all relevant features (CH_4, ambient N_2O, ambient H_2O, which is assumed to be 1%, verified by meteorological measurements and the N_2O reference signal). The 2f spectral fitting residuals are ~3% of the

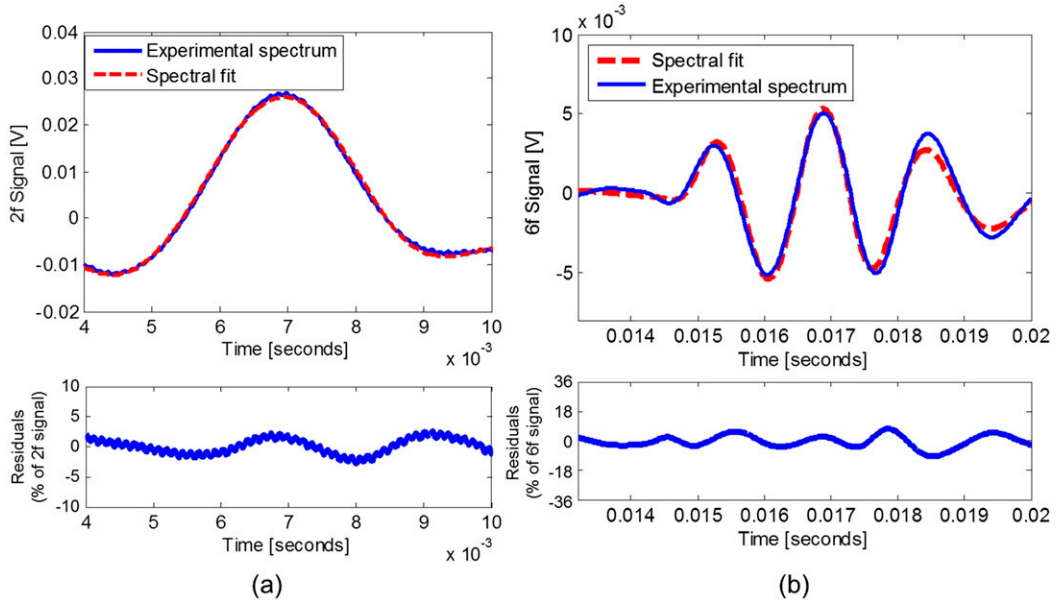

FIG. 4. (a) Ambient methane 2f signal (1-s averaging) recorded in the field at Toolik Lake along with the real-time fitted spectrum. Note the residuals of the spectral fit are plotted on a smaller voltage range than the ambient spectrum to better illustrate the spectral noise. (b) The 6f signal of N_2O reference cell signal recorded with 30-s averaging in the field at Toolik Lake, along with the real-time fitted spectrum and spectral fitting residuals.

CH_4 absorption signal height, and the 6f residuals are ~9% of the N_2O reference absorption signal height.

Although the occurrence of large CH_4 plumes within the long path would lead to nonlinear optical absorption and saturation, we do not assume that the 2f signal scales linearly with concentrations. We can correct all 2f signal retrievals for nonlinearity due to strong absorption using a logarithmic function based on direct absorption calibration of 2f retrievals and periodically collect the direct absorption spectra to further check for optical saturation. However, the relative variations of CH_4 above background levels were typically small (<1%) and within that range the fluctuations will be linear. Optical saturation would occur similarly whether it was a high concentration distributed evenly across the entire measurement path or whether one short segment contained a high concentration leading to optical saturation because we integrate over all CH_4 plumes along the path. For example, if a 1% mixing ratio (10 000 ppm) CH_4 point source occurred over 1 m of a 500-m total pathlength with ambient (2 ppmv CH_4) levels along the remainder of the measurement path, we would observe an integrated measurement of 11 000 ppmv m^{-1} and saturation of spectra would be clearly evident.

The open-path-integrated QC laser–based sensor mixing ratio retrievals were calibrated in the arctic field environment using seven air samples taken on the shoreline parallel to the laser path above the lake and analyzed offline in the laboratory using gas chromatography (GC). The air samples were calibrated with a NOAA Global Monitoring Division (GMD) standard (1.8724 ± 0.003 ppmv CH_4) and two commercial CH_4 standards. The total uncertainty in the calibration factor from these standards is ±2% based on the gas standard uncertainties. During the field intercomparison, CH_4 mixing ratios were calibrated to the LI-COR LI-7700 CH_4 analyzer measurements over a measurement range of ~300 ppbv CH_4 enhancements. These LI-COR CH_4 measurements were previously calibrated to the same NOAA GMD calibration standard.

3. Field sites

a. Toolik Lake, Alaska

The QC laser–based CH_4 sensor was deployed in August 2012 across Toolik Lake at the Toolik Field Station in Alaska (68°38′N, 149°36′W). During the measurement period, this site experienced a variety of field conditions, including precipitation (rain and snow) and high winds. The sensor was located inside a wooden shelter (~1 m × 1.5 m × 1 m) to protect it from precipitation events, wind, and insects. The input and output beams passed through a 15 cm × 15 cm opening in the shelter. Electronic line power was provided from a laboratory building at the field station. The sensor was deployed on the southern shoreline of Toolik Lake. The retroreflector, attached to a tripod, was placed at three locations across the lake separately (Fig. 5) to evaluate the sensor performance at round-trip optical pathlengths of 458, 756, and 1288 m. respectively. Alignment across the lake was achieved using the visible (532 nm) laser and a spotting scope. Both the visible and QC laser beams traversed across the lake at approximately 1 m above the water surface. High QC laser optical power and minimal laser beam divergence (0.35 mrad) were both critical for long-distance measurements.

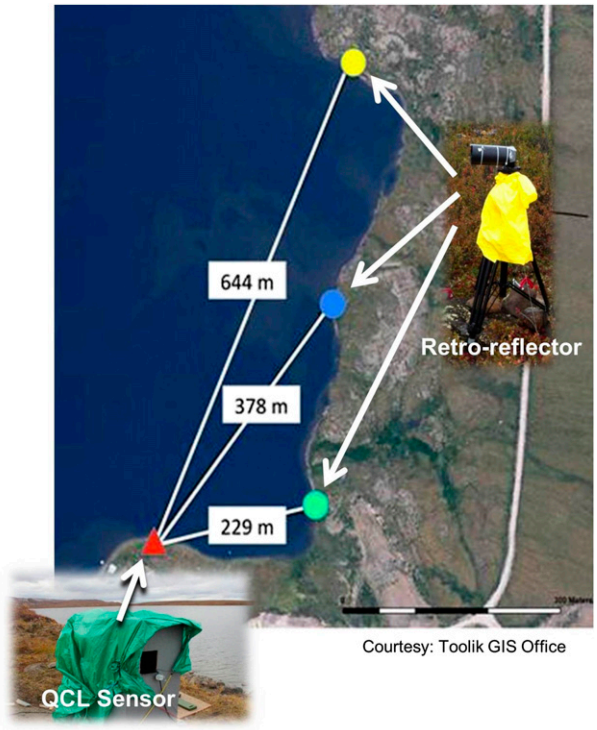

FIG. 5. Three long pathlengths (one-way distances displayed) implemented across Toolik Lake during the summer 2012 deployment. The retroreflector was deployed at the locations denoted by yellow, blue, and green points to achieve the pathlengths indicated during separate phases of the field campaign.

The ~1-m beam size allowed the effects of beam movement from scintillation to be minimized both at the retroreflector and at the collection optics (20.32-cm-diameter mirror). While scintillation was indeed occurring, it did not appear to be a driving factor on the alignment, as short-term fluctuations (1 Hz) in the detector signal were often well below 1%. Since the 2f WMS signal was normalized by the 1f dc value at the

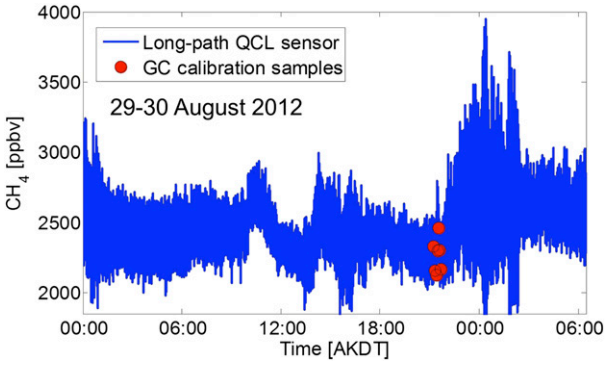

FIG. 6. Time series of 1-s CH_4 measurements at Toolik Lake. The 29–30 Aug 2012 data were obtained at 458-m pathlength. The seven calibration samples collected along the measurement path and analyzed by GC are also plotted during their respective collection times on 29 Aug 2012.

CH_4 absorption line center, the measurement was generally not sensitive to long-term (several minutes) drifts in light intensity (until the detector signal itself became noisy). In addition, the intensity of ambient light at 8 μm from ambient blackbody radiation did not impact our measurement for two reasons. First, the laser light reaching the detector was orders of magnitude above the in-field detector noise floor (which would nominally include ambient blackbody radiation). Second, we detect at high frequencies (40 kHz), whereas ambient 8-μm light is not modulated.

Relative humidity, air temperature, and pressure were measured with a digital temperature sensor (Innovative Sensor Technology HYT 271, ±0.2°C accuracy) and a digital pressure sensor (TE Connectivity MS5803-01BA, ±0.5-hPa accuracy) nearby on the shoreline. Although no corrections were applied to account for spectroscopic temperature effects on CH_4 spectral fitting routines, the reference cell temperature was measured in real time and used for spectral fitting of the N_2O reference signal. The spectroscopic temperature effects on the CH_4 signal were <1% for the range of temperatures (−1° to 19°C) observed during the field measurements.

b. *Broadmead, Princeton, New Jersey*

An intercomparison field experiment was conducted at the Princeton University Broadmead eddy covariance field site (40°20′46.9″N, 74°38′36.5″W) in Princeton, New Jersey, with a commercial open-path CH_4 analyzer (LI-COR LI-7700) designed for point (rather than path integrated) measurements (McDermitt et al. 2011). The LI-COR LI-7700 analyzer has a 1-s precision of 2 ppbv CH_4 and long-term drift (over hours) of ~20 ppbv CH_4. Meteorological data used in the analysis were obtained from routine measurements at the Princeton Broadmead eddy covariance field site. Ambient temperature and relative humidity were measured with a Campbell Scientific HMP45c temperature and relative humidity probe. Precipitation was measured with two Campbell Scientific CS700 tipping-bucket rain gauges in a dual-platform system. Results are discussed below.

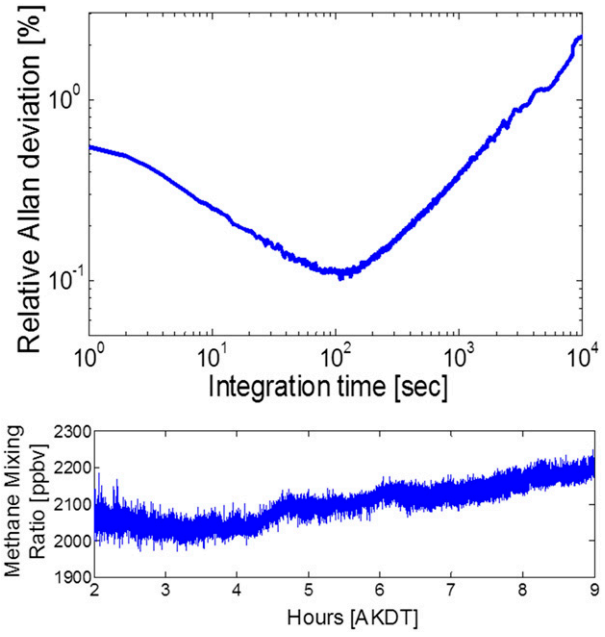

FIG. 7. Relative Allan deviation plot of ambient 1-s CH_4 data recorded over 7 h across Toolik Lake at a 458-m total (round-trip) pathlength. The horizontal axis is local time [Alaska daylight time (AKDT)] hours.

4. Field performance

a. *Deployment at Toolik Lake*

Figure 6 shows the time series of 1-s CH_4 measurements at Toolik Lake. Data on 29 and 30 August 2012 data were obtained at 458-m pathlength. The seven calibration samples collected along the measurement path and analyzed by gas chromatography are also plotted during their respective collection times on 29 August 2012.

We evaluate the short-term precision and long-term stability of the path-integrated CH_4 sensor using the Allan deviation method (Werle 2011). Figure 7 shows the Allan deviation plot for 1-s ambient CH_4 mixing ratios recorded for a 7-h period at Toolik Lake at 458-m optical pathlength with no reference cell present in the system. The relative Allan deviation was 0.5% at 1-s integration time, which is equivalent to ~10 ppbv CH_4. This is an upper limit to the actual sensor precision due to atmospheric CH_4 variability. The short-term

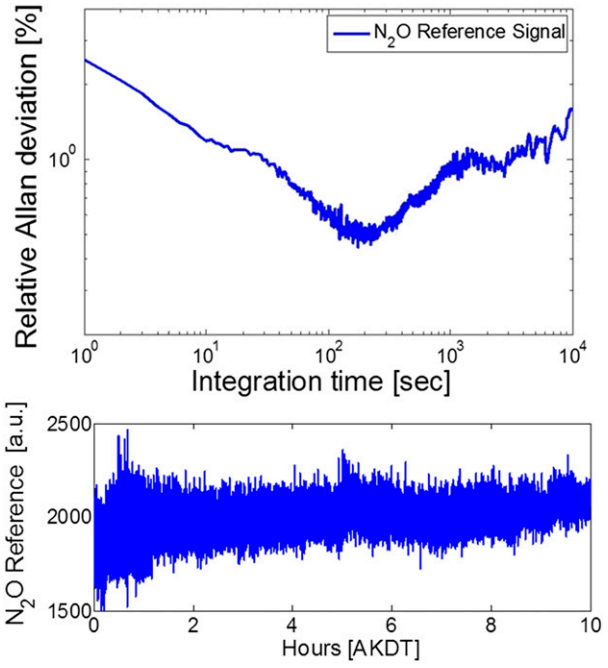

FIG. 8. Relative Allan deviation plot of in-line N_2O reference signal (1 s) recorded over 10 h in the field at Toolik Lake. The horizontal axis is local time (AKDT) hours.

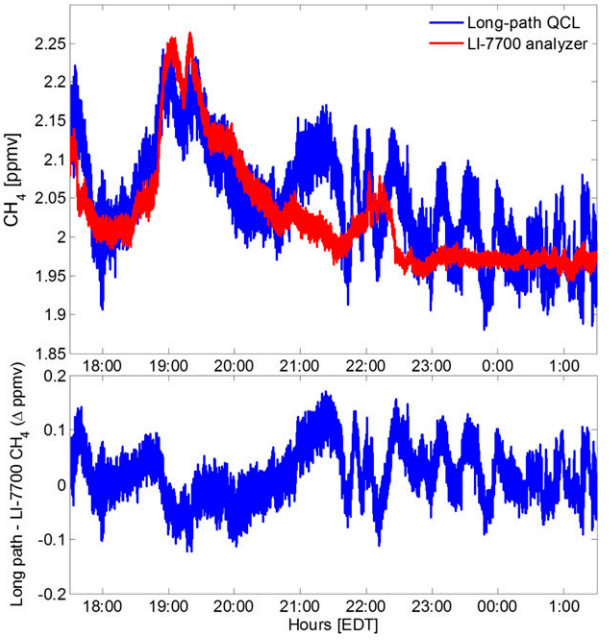

FIG. 9. (top) Time series of simultaneous 1-s CH_4 mixing ratio measurements by LI-COR LI-7700 and open-path-integrated QCL-based sensors. The open-path-integrated measurements are interpolated to the LI-COR data time stamps for comparison. (bottom) The difference or residuals of the 1-s data comparison. The horizontal axes are local time [eastern daylight time (EDT; hours:minutes)]. The data were taken on 16 and 17 Mar 2013. The reference cell was not in place during these measurements.

precision for measurements at the longest pathlength implemented (1.29 km round-trip) was degraded by ~25% compared with the precision at 458-m pathlength due to lower light intensity on the detector with a larger beam incident on the retroreflector at longer pathlengths.

On time scales longer than ~100 s, sensor drift leads to an increase in the Allan deviation (Fig. 7), suggesting that calibration is needed on these time scales to ensure accuracy. Figure 8 shows the relative Allan deviation plot of the raw 6f N_2O signal over a 10-h period in the field. The reference signal drift on time scales up to 10^4 s remains below the 1-s precision (2.5%). Based on the Allan deviation plot in Fig. 8, the in-line approach can account for a 1% instrument drift up to 1-h time scales. The 1-s precision of the 6f N_2O reference signal is worse than the 2f CH_4 precision due to the intrinsically lower signal-to-noise ratio of 6f signals. Therefore, 30-s averaging is applied to the N_2O signal to avoid additional noise contributions to the normalized CH_4 retrieval.

b. *Sensor intercomparison at Broadmead*

The open-path-integrated QC laser–based sensor and LI-COR LI-7700 point sensor were deployed at the Princeton Broadmead eddy covariance field site for simultaneous CH_4 measurements. The open-path-integrated QC laser–based sensor was aligned to a total (round-trip) pathlength of 240 m. The QC laser–based sensor was collocated with the LI-COR (shown in Fig. 1b). The Broadmead site includes a field and a detention pond, is surrounded on all four sides by roads, and is in very close proximity to Carnegie Lake. The deployment of the LI-COR allowed for the temporal variability in methane at one location at the site to be quantified, and given the nominal wind speed of ~1 m s^{-1}, this can be linked to show there is some spatial heterogeneity in the CH_4 concentration field at this site. With a nominal wind speed of 1 m s^{-1}, the transport of air across 120 m is ~120 s. Well-mixed conditions within the path are expected after ~5 times this transport time (after 10 min). Figure 9 shows 1-s measurements over >7 h on 16 and 17 March 2013 for both sensors during the field deployment. The reference cell was not in place during these measurements.

The reference cell was installed from 11 to 12 March during the first part of the Broadmead intercomparison study. A 1-s precision of 0.6% or ~11 ppbv CH_4 was achieved with the reference cell installed at the Broadmead site. For the second portion of the intercomparison period, the reference cell was removed to

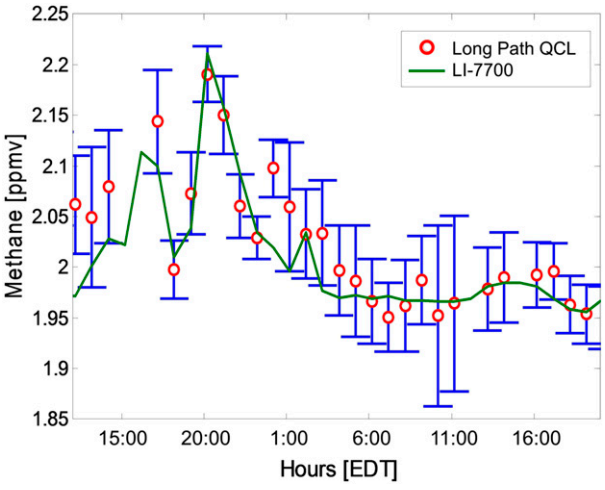

FIG. 10. Intercomparison of open-path-integrated QCL sensor and LI-COR LI-7700 analyzer at the Princeton Broadmead site with 1-h-averaged measurements. The error bars represent the standard deviation of 1-s measurements during the 1-h time averaging window. The horizontal axes are local time (EDT; hours: minutes). The data were taken on 16 and 17 Mar 2013. The reference cell was not in place during these measurements.

improve both the short-term precision (increase full-scale signal on the detector) and to evaluate whether stability could be improved by eliminating the potential source of optical fringing due to the uncoated reference cell windows. However, significant oscillations of CH_4 retrievals were still observed during the second portion of the study and attributed to both laser wavelength thermal drift and fringing resulting from other optical components in the system.

The time series indicates that both sensors captured a large enhancement in CH_4 mixing ratio from 1830 to 2030 eastern daylight time (EDT). During the overnight period after 2100 EDT, differences are seen in the CH_4 retrieval (with no reference signal normalization) of the QC laser–based sensor and the LI-COR. After 2300 EDT oscillations with a peak-to-peak maximum of 5%–10% appear, whereas the LI-COR measurements remain approximately constant. These oscillations with a period of ~25–30 min are apparent in the residuals plot (Fig. 9) and represent a clear instrument drift not apparent in the LI-COR measurements. During this period, the two retrievals are not correlated at 1-s time resolution (ρ = 0.14). Figure 10 shows 1-h-averaged measurements during the intercomparison study for the data shown in Fig. 9. To compare the two sensors, we utilize a 1-h average due to the differences in sampling footprints (to provide sufficient time averaging to allow for well-mixed conditions along the integrated path) and to average instrument drift. Nearly all 1-h-averaged LI-COR measurements fall within one standard deviation of the open-path-integrated measurements during each measurement hour. The oscillatory drifts at 25–30-min periods observed in the long-path sensor measurements both with and without the in-line reference cell installed suggest that improved laser temperature control and reduction in optical fringing are needed to maintain system stability. The drift observed in the long-path sensor signals both with and without the in-line reference cell installed suggests that improved laser temperature control and reduction in optical fringing are needed to maintain system stability. The nature of the drifts observed is consistent with evidence for optical fringing, mainly oscillation of the absorption retrieval for a system with some uncoated transmissive optics. These are widely observed evidence for optical fringing, which is the main stability limitation in many laser absorption spectrometers. In addition, we add that the oscillations without the reference cell correlated well in period and phase with the CH_4 absorption line center position, a proxy for laser wavelength. The main source of wavelength drift for quantum cascade lasers (QCLs) is temperature control of the heat sink.

c. *Field condition impacts on sensor stability at Toolik Lake and Broadmead Field sites*

We investigate the impacts of variable environmental conditions on the path-integrated sensor light intensity stability. During the deployment period at Toolik Lake, environmental conditions included a range of air temperatures (−1° to 19°C), snowfall (15.6-mm accumulation on 27 August), and variable wind speeds up to 9.3 m s^{-1}. Figure 11 shows the effects of snowfall and rainfall on the open-path-integrated sensor during the Princeton Broadmead site deployment. Although open-path measurement data quality may inevitably be degraded temporarily due to precipitation, a field sensor must be capable of autonomous operation through these precipitation events. The open-path-integrated sensor recovered light intensity without any intervention following a snowfall event (Fig. 11a). Moderate rainfall resulted in small attenuation of light intensity on the detector, which did not significantly degrade data quality for the first 5 h after the rainfall period began (Fig. 11b). However, the signal strength inevitably degraded significantly after a doubling of rain rate in the early afternoon. During the deployment period at Toolik Lake, heavy snowfall (not shown) resulted in the sensor losing signal primarily due to snow accumulation inside the retroreflector housing. With the addition of a precipitation shield on the retroreflector, the signal and data quality were recovered following the snowfall period.

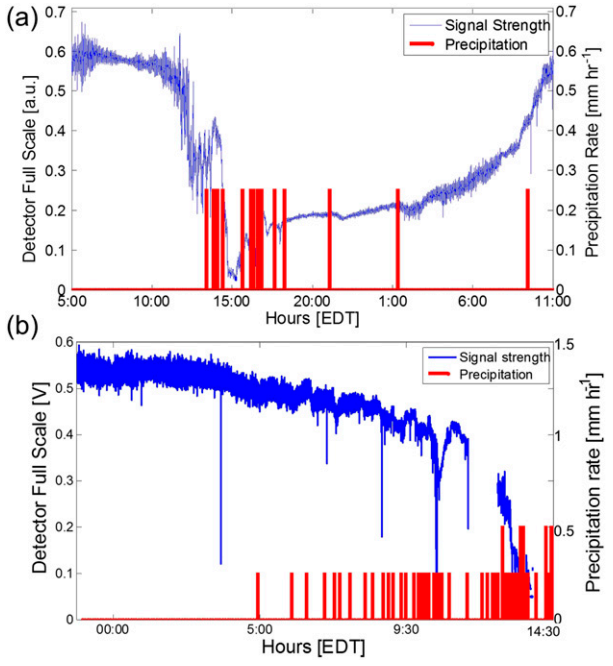

FIG. 11. (a) The effect of snowfall on the signal strength of the open-path-integrated QCL sensor at the Princeton Broadmead eddy covariance site in March 2013. (b) Effects of rainfall on the signal strength of the open-path-integrated QCL-based sensor at the Princeton Broadmead site.

5. Discussion

We demonstrate the performance of a path-integrated methane sensor in an extreme variable field environment. The in-line reference signal N_2O 6f provides an independent metric of system stability for the long-path measurement. While the 6f signal is inherently noisier than the 2f signal (by a factor of 10), integrating over longer times (minutes) recovers a comparable signal-to-noise ratio as the ambient 1-Hz CH_4 signal. For example, increased noise in the ambient methane signal is due to either an instrument problem or increase in real atmospheric variability. The in-line reference cell is useful to observe instrument noise, such as from the instability in the thermoelectric cooling of the laser or detector, which results in reference signal oscillations. The reference cell signal line center position variations were useful for diagnosing thermal drifts of the laser wavelength and for separating those from optical fringing. The ability to separate these aspects is particularly important for a field-based sensor that is largely exposed to the environment.

Future studies will focus on the improvement of overall stability beyond that achieved in this study with the in-line reference cell method. For example, optical fringes are a dominant source of drift in the 2f ambient CH_4 spectra and manifest themselves differently at the bandwidth and frequency of the sixth harmonic in-line reference signal. The phase, amplitude, and frequency of fringes are expected to show different behavior in the reference and ambient signals. Indeed, optical fringing is one major reason why the long-term stability of the CH_4 sensor drifted at percent levels during the field study. Ongoing efforts are examining different protocols to address some aspects of this and reducing the optical fringes themselves (e.g., better antireflectivity coating of the in-line reference cell itself and detector windows). The reference cell, detector, and laser housing were made with one choice of antireflectivity coating from the vendor. Since we observed significant fringes from the transmissive optics, alternative antireflectivity coatings will be implemented for future deployments. Because of time constraints, a different custom coating could not be obtained prior to the field campaign. Future refinements of the sensor system will improve precision and long-term drift by implementing custom antireflection coatings on all transmissive optical components and installing a beam expander to improve beam collimation at long pathlengths.

Atmospheric CH_4 mixing ratios were measured at an arctic lake site with potentially multiple local CH_4 sources nearby. Therefore, the precision of these heterogeneous measurements gives an upper limit to the instrument precision. The equivalent fractional absorbance for the 1-s (1-Hz bandwidth) precision at 458-m pathlength was 7×10^{-4}. Electronic noise from detector electronics limited the short-term precision. The beam divergence also limited the collection of all light on the retroreflector, further degrading the received light intensity and limiting short-term precision.

The QC laser–based long-path sensor shows excellent field precision and reasonable stability. However, for detecting even small and distributed emissions, improved stability and precision are needed. Optical fringing (which largely defines the sensor drift) needs to be reduced, and improved coatings on the reference cell itself are needed. We note, however, that upon going well below 1% precision/stability, other correction factors are needed, such as water vapor effects (spectroscopic and dilution), temperature inhomogeneities, and knowledge of wind velocities.

6. Summary and future applications

We developed and field tested the first long-path sensor using a QC laser to achieve high-precision CH_4 measurements in the Arctic, a demanding, harsh environment. We also demonstrated the sensor at Broadmead Field in Princeton, New Jersey. Robust field

measurement capabilities were demonstrated, including operation during snowfall and rainfall events. By coupling a QC laser with an in-line reference cell, we demonstrated that the sensor could measure CH_4 in the Arctic, a challenging field site. High-precision (0.5% in 1 s) CH_4 mixing ratio retrievals were achieved as a result of the sensor being designed to operate in a highly variable, harsh environment. The relative Allan deviation of 0.5% at 1-s integration time is equivalent to ~10 ppbv CH_4 and as stated earlier is an upper limit to the actual sensor precision as a result of real atmospheric CH_4 variability.

In field tests at Princeton University, the open-path-integrated sensor intercompared well with a commercial CH_4 sensor with 1-h averaging and captured large variations in ambient mixing ratios. Future designs will incorporate several refinements to address the noise and drift sources discussed above, as well as miniaturization and weatherproofing.

In a broader context, the open-path-integrated CH_4 sensor design may be generalized to other trace gases detected at different wavelengths than 8 μm. However, in order to extend this design to other lasers targeting other gases, numerous considerations would need to be made. For some other gases, the stability needed for robust measurements may be significantly less than required here for methane. The main considerations for implementing this system for other trace gases would be accounting for potential optical saturation near large source regions at kilometer-scale pathlengths, sufficient laser optical power (ideally tens of megawatts), beam collimation for receiving adequate optical power, custom optical coatings for the detection wavelength, and the appropriate reference gas choice based on nearby absorption lines offset from the absorption line of interest for ambient detection.

The path-integrated laser-based CH_4 sensor technology is directly applicable to characterize CH_4 emissions using CH_4 mixing ratio gradients at different heights above ground in the vicinity of many anthropogenic and natural CH_4 sources. The open-path-integrated sensing platform is especially advantageous for spatially heterogeneous and temporally variable CH_4 sources with large uncertainties, including agricultural emissions and petrochemical activities ranging from natural gas infrastructure leakage to hydraulic fracturing wells and waste facilities (Howarth et al. 2011; Alvarez et al. 2012; Peischl et al. 2012; Péron et al. 2012; Karion et al. 2013; Miller et al. 2013). Finally, open-path-integrated CH_4 measurements at long (kilometer) pathlengths can also be used to detect emissions for comparison with CH_4 model simulations and emission inventories on comparable spatial scales.

Acknowledgments. The authors gratefully acknowledge funding for this work by MIRTHE through NSF-ERC Grant EEC-0540832. The authors wish to thank Professor Claire F. Gmachl and her research group and Professor James Smith and his research group for the valuable support and feedback. We specifically thank Mary Lynn Baeck for access to the Princeton University Broadmead site for field measurements and the supporting meteorological data from the site. We also thank Matthew Reid for assisting with the GC measurements and Victor Fu for work on the initial sensor development and field testing, and LI-COR Biosciences for use of the LI-7700 CH_4 analyzer. Finally, we are grateful for the help and support of the NSF Toolik Field Station staff for use of their facilities and for logistical assistance with the field measurements in Alaska. D. J. Miller acknowledges support by the National Science Foundation Graduate Research Fellowship under Grant DGE-0646086. K. Sun acknowledges support by the NASA Earth and Space Science Fellowship IIP-1263579.

REFERENCES

Alvarez, R., S. Pacala, J. Winebrake, W. Chameides, and S. Hamburg, 2012: Greater focus needed on methane leakage from natural gas infrastructure. *Proc. Natl. Acad. Sci. USA*, **109**, 6435–6440, doi:10.1073/pnas.1202407109.

Anderson, B., K. B. Bartlett, S. Frolking, K. Hayhoe, J. C. Jenkins, and W. A. Salas, 2010: Methane and nitrous oxide emissions from natural sources. U.S. EPA Office of Atmospheric Programs Rep. 430-R-10-001, 196 pp.

Bacsik, Z., J. Mink, and G. Keresztury, 2005: FTIR spectroscopy of the atmosphere part 2. Applications. *Appl. Spectrosc. Rev.*, **40**, 327–390, doi:10.1080/05704920500230906.

Brooke, J., and Coauthors, 2012: Greenhouse gas measurements over a 144 km open path in the Canary Islands. *Atmos. Meas. Tech.*, **5**, 2309–2319, doi:10.5194/amt-5-2309-2012.

Childers, J., E. L. Thompson Jr., D. Harris, D. Kirchgessner, M. Clayton, D. Natschke, and W. Phillips, 2001: Multipollutant concentration measurements around a concentrated swine production facility using open-path FTIR spectrometry. *Atmos. Environ.*, **35**, 1923–1936, doi:10.1016/S1352-2310(00)00545-8.

Cole, J., and Coauthors, 2007: Plumbing the global carbon cycle: Integrating inland waters into the terrestrial carbon budget. *Ecosystems*, **10**, 172–185, doi:10.1007/s10021-006-9013-8.

Demirgian, J., and S. Macha, 1999: Collection of quantitative chemical release field data. *Field Anal. Chem. Technol.*, **3**, 95–104, doi:10.1002/(SICI)1520-6521(1999)3:2<95::AID-FACT4>3.0.CO;2-G.

Desjardins, R., O. Denmead, L. Harper, M. McBain, D. Masse, and S. Kaharabata, 2004: Evaluation of a micrometeorological mass balance method employing an open-path laser for measuring methane emissions. *Atmos. Environ.*, **38**, 6855–6866, doi:10.1016/j.atmosenv.2004.09.008.

Dlugokencky, E., E. Nisbet, R. Fisher, and D. Lowry, 2011: Global atmospheric methane: Budget, changes and dangers. *Philos. Trans. Roy. Soc. London*, **369**, 2058–2072, doi:10.1098/rsta.2010.0341.

Eugster, W., and P. Pluss, 2010: A fault-tolerant eddy covariance system for measuring CH_4 fluxes. *Agric. For. Meteor.*, **150**, 841–851, doi:10.1016/j.agrformet.2009.12.008.

Farrell, P., D. Culling, and I. Leifer, 2013: Transcontinental methane measurements: Part 1. A mobile surface platform for source investigations. *Atmos. Environ.*, **74**, 422–431, doi:10.1016/j.atmosenv.2013.02.014.

Flesch, T., J. Wilson, L. Harper, R. Todd, and N. Cole, 2007: Determining ammonia emissions from a cattle feedlot with an inverse dispersion technique. *Agric. For. Meteor.*, **144**, 139–155, doi:10.1016/j.agrformet.2007.02.006.

Garcia-Tigreros Kodovska, F. G.-T., K. J. Sparrow, S. A. Yvon-Lewis, A. Paytan, N. T. Dimova, A. Lecher, and J. D. Kessler, 2016: Dissolved methane and carbon dioxide fluxes in Subarctic and Arctic regions: Assessing measurement techniques and spatial gradients. *Earth Planet. Sci. Lett.*, **436**, 43–55, doi:10.1016/j.epsl.2015.12.002.

Gibson, G., B. van Well, J. Hodgkinson, R. Pride, R. Strzoda, S. Murray, S. Bishton, and M. Padgett, 2006: Imaging of methane gas using a scanning, open-path laser system. *New J. Phys.*, **8**, 26, doi:10.1088/1367-2630/8/2/026.

Griffith, D., and B. Galle, 2000: Flux measurements of NH_3, N_2O and CO_2 using dual beam FTIR spectroscopy and the flux–gradient technique. *Atmos. Environ.*, **34**, 1087–1098, doi:10.1016/S1352-2310(99)00368-4.

Howarth, R., R. Santoro, and A. Ingraffea, 2011: Methane and the greenhouse gas footprint of natural gas from shale formations. *Climatic Change Lett.*, **106**, 679–690, doi:10.1007/s10584-011-0061-5.

IPCC, 2013: *Climate Change 2013: The Physical Science Basis*. Cambridge University Press, 1535 pp., doi:10.1017/CBO9781107415324.

Isaksen, I., M. Gauss, G. Myhre, K. W. Anthony, and C. Ruppel, 2011: Strong atmospheric chemistry feedback to climate warming from Arctic methane emissions. *Global Biogeochem. Cycles*, **25**, GB2002, doi:10.1029/2010GB003845.

Karion, A., and Coauthors, 2013: Methane emissions estimate from airborne measurements over a western United States natural gas field. *Geophys. Res. Lett.*, **40**, 4393–4397, doi:10.1002/grl.50811.

McDermitt, D., and Coauthors, 2011: A new low-power, open-path instrument for measuring methane flux by eddy covariance. *Appl. Phys.*, **102A**, 391–405, doi:10.1007/s00340-010-4307-0.

Michel, A. P., and Coauthors, 2010: Quantum cascade laser open-path system for remote sensing of trace gases in Beijing, China. *Opt. Eng.*, **49**, 111125, doi:10.1117/1.3509316.

Miller, D., K. Sun, L. Tao, M. Khan, and M. Zondlo, 2014: Open-path, quantum cascade-laser-based sensor for high-resolution atmospheric ammonia measurements. *Atmos. Meas. Tech.*, **7**, 81–93, doi:10.5194/amt-7-81-2014.

Miller, S., and Coauthors, 2013: Anthropogenic emissions of methane in the United States. *Proc. Natl. Acad. Sci. USA*, **110**, 20 018–20 022, doi:10.1073/pnas.1314392110.

Montzka, S., E. Dlugokencky, and J. Butler, 2011: Non-CO_2 greenhouse gases and climate change. *Nature*, **476**, 43–50, doi:10.1038/nature10322.

Peischl, J., and Coauthors, 2012: Airborne observations of methane emissions from rice cultivation in the Sacramento Valley of California. *J. Geophys. Res.*, **117**, D00V25, doi:10.1029/2012JD017994.

Peltola, O., I. Mammarella, S. Haapanala, G. Burba, and T. Vesala, 2013: Field intercomparison of four methane gas analysers suitable for eddy covariance flux measurements. *Biogeosciences*, **10**, 3749–3765, doi:10.5194/bg-10-3749-2013.

Pétron, G., and Coauthors, 2012: Hydrocarbon emissions characterization in the Colorado Front Range: A pilot study. *J. Geophys. Res.*, **117**, D04304, doi:10.1029/2011JD016360.

Rigby, M., and Coauthors, 2008: Renewed growth of atmospheric methane. *Geophys. Res. Lett.*, **35**, L22805, doi:10.1029/2008GL036037.

Rothman, L., and Coauthors, 2009: The *HITRAN* 2008 molecular spectroscopic database. *J. Quant. Spectrosc. Radiat. Transfer*, **110**, 533–572, doi:10.1016/j.jqsrt.2009.02.013.

Schilt, S., L. Thévenaz, and P. Robert, 2003: Wavelength modulation spectroscopy: Combined frequency and intensity laser modulation. *Appl. Opt.*, **42**, 6728–6738, doi:10.1364/AO.42.006728.

Sun, K., L. Tao, D. Miller, M. Khan, and M. Zondlo, 2013: In-line multi-harmonic calibration method for open-path atmospheric ammonia measurements. *Appl. Phys.*, **110B**, 213–222, doi:10.1007/s00340-012-5231-2.

Suto, H., and G. Inoue, 2010: A new portable instrument for in situ measurement of atmospheric methane mole fraction by applying an improved tin dioxide–based gas sensor. *J. Atmos. Oceanic Technol.*, **27**, 1175–1184, doi:10.1175/2010JTECHA1400.1.

Tao, L., K. Sun, M. Khan, D. Miller, and M. Zondlo, 2012: Compact and portable open-path sensor for simultaneous measurements of atmospheric N_2O and CO using a quantum cascade laser. *Opt. Express*, **20**, 28 106–28 118, doi:10.1364/OE.20.028106.

Thoma, E., and Coauthors, 2005: Open-path tunable diode laser absorption spectroscopy for acquisition of fugitive emission flux data. *J. Air Waste Manage. Assoc.*, **55**, 658–668, doi:10.1080/10473289.2005.10464654.

Walter, K. M., L. C. Smith, and F. S. Chapin III, 2007: Methane bubbling from northern lakes: Present and future contributions to the global methane budget. *Philos. Trans. Roy. Soc. London*, **365A**, 1657–1676, doi:10.1098/rsta.2007.2036.

Walter-Anthony, K. M., and P. Anthony, 2013: Constraining spatial variability of methane ebullition seeps in thermokarst lakes using point process models. *J. Geophys. Res. Biogeosci.*, **118**, 1015–1034, doi:10.1002/jgrg.20087.

Werle, P., 2011: Accuracy and precision of laser spectrometers for trace gas sensing in the presence of optical fringes and atmospheric turbulence. *Appl. Phys.*, **102B**, 313–329, doi:10.1007/s00340-010-4165-9.

Xia, H., and Coauthors, 2008: An approach of open-path gas sensor based on tunable diode laser absorption spectroscopy. *Chin. Opt. Lett.*, **6**, 437–440.